Probing the impact of chromatin conformation on genome editing tools

Xiaoyu Chen, Marrit Rinsma, Josephine M. Janssen, Jin Liu, Ignazio Maggio and Manuel A.F.V. Gonçalves[*]

Department of Molecular Cell Biology, Leiden University Medical Center, Einthovenweg 20, 2333 ZC, Leiden, The Netherlands

ABSTRACT

Transcription activator-like effector nucleases (TALENs) and RNA-guided nucleases derived from clustered, regularly interspaced, short palindromic repeats (CRISPR)-Cas9 systems have become ubiquitous genome editing tools. Despite this, the impact that distinct high-order chromatin conformations have on these sequence-specific designer nucleases is, presently, ill-defined. The same applies to the relative performance of TALENs and CRISPR/Cas9 nucleases at isogenic target sequences subjected to different epigenetic modifications. Here, to address these gaps in our knowledge, we have implemented quantitative cellular systems based on genetic reporters in which the euchromatic and heterochromatic statuses of designer nuclease target sites are stringently controlled by small-molecule drug availability. By using these systems, we demonstrate that TALENs and CRISPR/Cas9 nucleases are both significantly affected by the high-order epigenetic context of their target sequences. In addition, this outcome could also be ascertained for *S. pyogenes* CRISPR/Cas9 complexes harbouring Cas9 variants whose DNA cleaving specificities are superior to that of the wild-type Cas9 protein. Thus, the herein investigated cellular models will serve as valuable functional readouts for screening and assessing the role of chromatin on designer nucleases based on different platforms or with different architectures or compositions.

INTRODUCTION

Transcription activator-like effector (TALE) nucleases (TALENs) and RNA-guided clustered, regularly interspaced, short palindromic repeats (CRISPR)-associated Cas9 (CRISPR/Cas9) nucleases, have become the prevalent tools for inducing targeted double-stranded DNA breaks (DSBs) in living cells ([1,2]).

Native TALE proteins have evolved in phytopathogenic bacteria (*Xanthomonas* sp.) to serve as transcriptional activators of specific host plant genes whose products promote infection ([1,2]). Typically, TALE DNA-binding domains consist of an array of 15.5–19.5 repeats composed of 33–34 residues containing polymorphisms called repeat variable di-residues (RVDs) at positions 12 and 13. Individual RVDs mediate the binding of the repeat in which they are embedded to a particular nucleotide. This direct one-to-one interaction between nucleotides and repeats permits the straightforward assembling of artificial proteins, among which TALENs, with specific DNA binding activities. Indeed, TALENs are built by fusing the DNA-binding programmable polymorphic repeats from TALE proteins to the nuclease domain of the type IIS restriction enzyme FokI ([1,2]). The recognition of preselected genomic sequences by TALEN pairs leads to *in situ* FokI dimerization resulting in nuclease activation and targeted DSB formation.

Native CRISPR/Cas9 nucleases have evolved in bacteria and archaea as adaptive immune systems to fend off invading nucleic acids (e.g. bacteriophage and plasmid DNA) whose chromatin signatures are, clearly, fundamentally different from those present in and acquired by eukaryotic nuclear genes ([3]). Programmable CRISPR/Cas9 nucleases are ribonucleoprotein complexes composed of a sequence-tailored single guide RNA (gRNA) and a Cas9 protein harboring two nuclease domains (i.e. RuvC and HNH). The 5′ and 3′ ends of the gRNAs serve as targeting and scaffolding moieties for Cas9, respectively. The initial interaction between CRISPR/Cas9 complexes and DNA involves binding of Cas9 to a nucleotide sequence named protospacer adjacent motif (PAM; NGG in the case of the prototypic Cas9 from *S. pyogenes*). This initial engagement with DNA is mediated through a composite PAM-interacting domain located in two regions of the Cas9 protein ([4]). Subsequently, targeted DSB formation is triggered after the hybridization of the 5′ end of the gRNA to a complementary ~20-bp genomic target sequence located next to the PAM ([1,2]).

---

[*]To whom correspondence should be addressed. Tel: +31 071 5269237; Email: M.Goncalves@lumc.nl

Therefore, TALENs and CRISPR/Cas9 nucleases operate in strikingly different manners in that the target site specificity of the former is governed via protein–DNA interactions, whilst that of the latter is ultimately dictated by RNA–DNA hybridizations (1,2). The activation of cellular DNA repair pathways resulting from the activity of these sequence-specific designer nucleases is being harnessed in an ever-increasing number of genome editing settings. For instance, the repair of targeted DSBs via non-homologous end joining (NHEJ) can result in the incorporation of small insertions and deletions (indels) leading to gene knock-out or gene correction (1,2).

Well-defined parameters that can affect targeted DSB formation by TALENs and CRISPR/Cas9 nucleases *in cellula* include their specific construction, composition, primary target sequence and, in the case of TALENs, CpG methylation (5,6). In contrast, there has been no direct and quantitative assessment of the impact that high-order chromatin conformations have on these gene-editing tools at isogenic target sites (7). By the same token, an investigation of the relative performance of TALENs and CRISPR/Cas9 nucleases at target sequences subjected to different epigenetic modifications is equally lacking. Indeed, hitherto, studies based mostly on catalytically 'dead' Cas9 enzymes have exclusively correlated preferential interactions of CRISPR/Cas9 complexes with open chromatin regions bearing candidate off-target sites (e.g. 5-nucleotide seed sequences followed by the *S. pyogenes*'s PAM) (7–11). In this regard, it is also of note that binding of CRISPR/Cas9 complexes to DNA is, for the most part, uncoupled from actual phosphodiester bond cleavage (7,8,11). Here, to cover these gaps in our knowledge, we have adapted and validated cellular systems for tracking and measuring the impact of the epigenetically regulated three-dimensional chromatin structure on gene editing processes. By using these reporter systems, we demonstrate that TALENs and CRISPR/Cas9 nucleases are both significantly hindered by the chromatin context in which their target sequences are embedded.

MATERIALS AND METHODS

Recombinant DNA

The lentiviral transfer plasmid AD12_pLV.TetO.TLR.TetO (Supplementary Figure S1) was constructed by inserting tTR-KRAB binding elements upstream and downstream of the *TLR* construction (12) in pCVL Traffic Light Reporter 1.1 (Sce target) Ef1a Puro (Addgene plasmid #31482, herein referred to as pLV.TLR) by using standard recombinant DNA techniques. The lentiviral transfer plasmid pLVCT-tTR-KRAB (13) used to assemble LVCT-tTR-KRAB vector particles for the generation of reporter cells HEK.EGFP^TetO.KRAB, was obtained from Addgene (#11643). Likewise for the TALEN expression plasmids TAL2050 (#39408), TAL2051 (#39409), TAL2072 (#39442), TAL2073 (#39443), TAL2076 (#39446), TAL2077 (#39447), TAL2094 (#39428) and TAL2095 (#39429) encoding, respectively, TALEN-26-L, TALEN-26-R, TALEN-43-L, TALEN-43-R, TALEN-45-L, TALEN-45-R, TALEN-36-L and TALEN-36-R proteins based on the *Xanthomonas axonopodis* pv. *citri*

TALE scaffold (14). The TALEN expression plasmids AR36_pTALEN-GA-L and AR37_pTALEN-GA-R code for, respectively, TALEN-L^EGFP and TALEN-R^EGFP (15); herein referred to as TALEN-GA-L and TALEN-GA-R, respectively. The TALEN-GA-L and TALEN-GA-R proteins are based on the *Xanthomonas campestris* pv. *armoraciae* TALE scaffold and were custom-designed by GeneArt Gene Synthesis (ThermoFisher Scientific). The expression plasmid hCas9 (16); herein referred to as pCMV.Cas9, contains a human codon-optimized ORF coding for the *Streptococcus pyogenes* Cas9 nuclease (Addgene plasmid #41815). The gRNA acceptor plasmid S7_pUC.U6.sgRNA.Bvel-stuffer has a U6 RNA Pol III promoter for driving gRNA expression and was constructed as follows. The construct pLKO.1-puro.U6.sgRNA.BfuAI.stuffer (17) (Addgene plasmid #50920) was treated with BclI and, subsequently, with the Klenow fragment (both from ThermoFisher Scientific). Next, this vector backbone was dephosphorylated with FastAP (ThermoFisher Scientific) and ligated to a Klenow fragment-blunted 3431-bp *DMD* cDNA fragment harboring four BveI sites. This fragment was isolated after digesting pDysE (18) with EcoRI (ThermoFisher Scientific). Of note, the presence of extra BveI sites aids in achieving complete BveI digestion of the respective gRNA acceptor plasmid. These manoeuvres yielded AA19_pLKO.1-puro.U6.sgRNA.BveI-stuffer (Supplementary Figure S2). Finally, after digesting AA19_pLKO.1-puro.U6.sgRNA.BveI-stuffer with BveI (ThermoFisher Scientific) and EcoRI, the resulting 3822-bp insert was ligated to a 2676-bp fragment obtained by treating cloning vector pUCBM21 (Boehringer Mannheim) with HincII (ThermoFisher Scientific) and EcoRI. This cloning step led to the generation of gRNA acceptor plasmid S7_pUC.U6.sgRNA.Bvel-stuffer (Supplementary Figure S3). The expression plasmids coding for gRNA^TLR, gRNA^GFP2, gRNA^GFP3, gRNA^GFP4, gRNA^GFP5, gRNA^GFP6 and gRNA^GFP7 were assembled by inserting annealed oligonucleotide pairs 5′-ACCGGTGAGCTCTTATTTGCGTA-3′/5′-AAACT ACGCAAATAAGAGCTCAC-3′, 5′-ACCGCTGCC GTCCTCGATGTTG-3′/5′-AAACCAACATCGAGG ACGGCAG-3′, 5′-ACCGCCGTCCTCGATGTTGTG G-3′/5′-AAACCCACAACATCGAGGACGG-3, 5′-A CCGGGCACGGGCAGCTTGCCGG-3′/ 5′-AAACC CGGCAAGCTGCCCGTGCC-3′, 5-ACCGTCGCCCT CGAACTTCACCT-3′/ 5′-AAACAGGTGAAGTTCGA GGGCGA-3′, 5′-ACCGTAGGTCAGGGTGGTCAC GA-3′/ 5′-AAACTCGTGACCACCCTGACCTA-3′ an d 5′-ACCGGCGAGGGCGATGCCACCTA-3′/ 5′-AAA CTAGGTGGCATCGCCCTCGC-3′ into BveI-digested S7_pUC.U6.sgRNA.Bvel-stuffer, respectively.

The *EGFP* target sequences for gRNA^GFP4, gRNA^GFP5, gRNA^GFP6 were described previously as NGG site 1, NGG site 2 and NGG site 3, respectively (19). The target sequence for gRNA^GFP7 was also described before (20). The construct gRNA_GFP_T2 (17) expressing the herein named gRNA^GFP1 was obtained from Addgene (plasmid #41820). Plasmid gRNA_Cloning Vector expressing the herein called gRNA^Empty (Addgene plasmid #41824) and plasmid AM51_ pUC.U6.gRNA^NT encoding, respec-

tively, no gRNA and an irrelevant, non-targeting, gRNA, were used to serve as negative controls. The AM51_pUC.U6.gRNA^NT construct was generated by cloning into BveI-digested S7_pUC.U6.sgRNA.BveI-stuffer the annealed oligonucleotide pair 5′-ACCGGTGAGCTCTTAT TTGCGTAGCTAGCTGAC-3′/ 5′-AAACGTCAGCTA GCTACGCAAATAAGAGCTCAC-3′.

The generation of the isogenic set of expression plasmids encoding wild-type Cas9, SpCas9-HF1 (19) and eSpCas9(1.1) (21) was done as follows. The plasmid C55_pU.CAG.hrGFP.rBGpA (Supplementary Figure S4) was first digested with NotI and HincII, to remove the *hrGFP* ORF, after which the 5019-bp backbone fragment was extracted from the agarose gel. Next, the backbone was blunted and dephosphorylated by using the Klenow Fragment of the *E. coli* DNA polymerase I and FastAP, respectively (both from Thermo Fisher Scientific). The constructs VP12 (Addgene plasmid #72247) (19) and eSpCas9(1.1) (Addgene plasmid #71814) (21) encode the high-specificity Cas9 variants SpCas9-HF1 and eSpCas9(1.1), respectively. The ORFs coding for wild-type Cas9, SpCas9-HF1 and eSpCas9(1.1) were isolated from agarose gel after double digesting pCMV.Cas9 (16), VP12 and eSpCas9(1.1) with XbaI/MssI, NotI/MssI and AseI/EcoRI, respectively. The insert fragments corresponding to Cas9, SpCas9-HF1 and eSpCas9(1.1) were then blunted and ligated to the aforementioned plasmid backbone yielding expression plasmids AV62_pCAG.Cas9.rBGpA, AV64_pCAG.SpCas9-HF1.rBGpA and AW01_pCAG.eSpCas9(1.1).rBGpA, respectively.

Cells

HEK293T cells (American Type Culture Collection) and HEK293T cell-derived clone HEK.EGFP^TetO.KRAB were cultured as indicated elsewhere (22). HER.TLR^TetO.KRAB cells and their control *TetO*-negative counterparts HER.TLR^KRAB cells were maintained in DMEM supplemented with 10% fetal bovine serum (FBS), 10 mM MgCl_2 and hygromycin B (ThermoFisher Scientific) at a final concentration of 45 μg/ml. These cells were stably transfected with a tTR-KRAB expression plasmid based on the pcDNA3.1/Hygro(+) backbone (Life Technologies). The various cell types were kept at 37°C in a humidified-air 10% CO_2 atmosphere.

Lentiviral vectors

The generation of lentiviral vectors LVCT-tTR-KRAB, LV.TetO.TLR.TetO and LV.TLR was done by transfecting, respectively, pLVCT-tTR-KRAB, pLV.TetO.TLR.TetO and pLV.TLR into HEK293T cells together with packaging construct psPAX2 (Addgene #12260) and pseudotyping plasmid pLP/VSVG (Life Technologies), essentially as described in detail elsewhere (23,24).

Experimental models

The single cell-derived clone HEK.EGFP^TetO.KRAB, harboring a tTR-KRAB-regulated *EGFP* allele, was generated by transducing HEK293T cells with LVCT-tTR-KRAB.

In brief, 5×10^4 cells were seeded in wells of 24-well plates (Greiner Bio-One). After 24 h, the cells were exposed to 1, 0.5, 0.25, 0.125 and 0.062 Hela cell-transducing units (HTU)/cell of LVCT-tTR-KRAB. At 48 h post-transduction, the cells exposed to each vector multiplicity of infection (MOI) were split into wells of 6-well plates (Greiner Bio-One). At 6 days after transduction, these cells were either kept in regular culture medium or in culture medium supplemented with 500 ng/ml doxy-cycline (Dox). Three days later EGFP-directed flow cytometry analysis was carried out. The cell culture transduced with an MOI of 0.125 HTU/cell contained 6.9% and 0.34% of EGFP-positive cells in the presence and absence of Dox, respectively. This cell culture was selected for isolating LVCT-tTR-KRAB-transduced clones by adding 200 μl of a cell suspension with a concentration of 1.5 cells/ml into wells of 96-well plates (Greiner Bio-One). To increase the cloning efficiency, the culture medium was supplemented with 50 μM of α-thioglycerol and 20 nM of bathocuprine disulphonate (both from Sigma-Aldrich) (25). Analysis of Dox-dependent epigenetic regulation of target sequences in individual LVCT-tTR-KRAB-transduced clones by flow cytometry led to the selection of reporter cell clone HEK.EGFP^TetO.KRAB, which was kept in the presence of Dox (200 ng/ml) where indicated. The HER.TLR^TetO.KRAB and the control HER.TLR^KRAB reporter cells were generated by transducing HER clone A2 with LV.TetO.TLR.TetO and LV.TLR particles, respectively. Clone A2 is derived from PER.C6 cells (26) and expresses, in a constitutive fashion, tTR-KRAB from a stably integrated pcDNA3.1/Hygro(+) backbone (Life Technologies). In brief, 2×10^5 A2 cells were seeded in wells of 24-well plates (Greiner Bio-One). One day later, 4-fold serial dilutions of LV.TetO.TLR.TetO and LV.TLR clarified supernatant were applied onto the cells. At 48 h post-transduction, the cells were transferred to wells of 6-well plates. At approximately 2 weeks post-transduction, hygromycin (45 μg/ml) and Dox (200 ng/ml) were added into LV.TetO.TLR.TetO transduced cells. The addition of Dox allowed one week later the start of cell selection with puromycin at a final concentration of 1 μg/ml. LV.TLR transduced cells were exposed to hygromycin and puromycin. After 2 weeks in selection medium, puromycin-resistant polyclonal cell populations were expanded for carrying out transfection experiments and, where indicated, kept in the presence of Dox (500 ng/ml).

DNA transfections

Transfections were started by mixing each of the relevant plasmids and 1 mg/ml polyethyleneimine (PEI, Polysciences) in 50 μl of a 150 mM NaCl solution (Supplementary Tables S1–S4). These transfections were done in cells cultured in the absence or in the presence of Dox. In addition, for determining gene delivery efficiencies, all transfection mixtures contained a reporter-encoding plasmid. After around 10 s of vigorous vortexing, the DNA-PEI complexes were incubated at room temperature for 15 min and were subsequently directly applied into the medium of the target cells that had been seeded one day before. After 6–8 h, the transfection mixtures were removed and fresh reg-
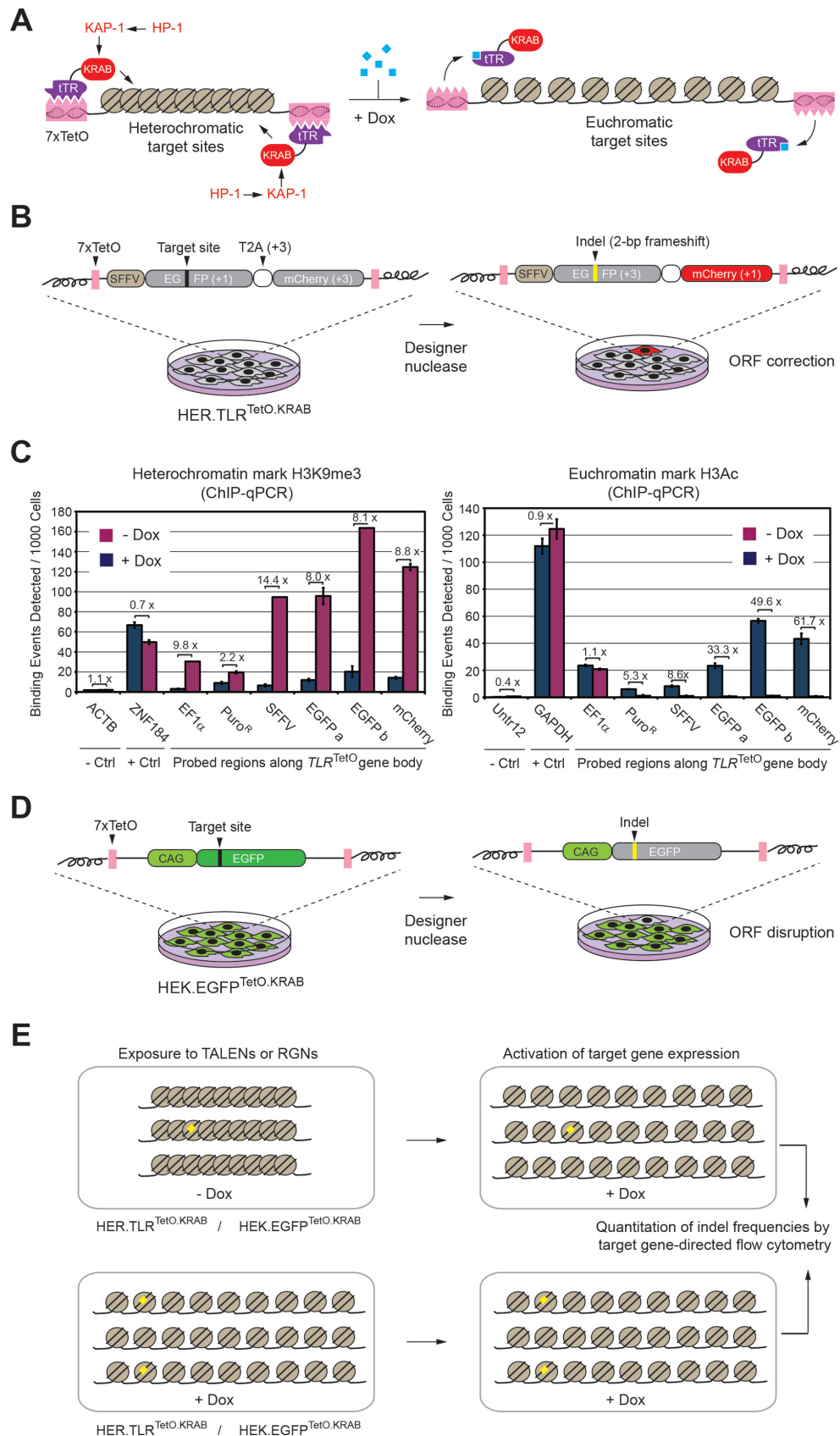
Figure 1. Experimental systems for tracking designer nuclease-induced indel formation at target sites with alternate epigenetic states. (**A**) Drug-dependent control over the chromatin conformation of designer nuclease target sites. In this system, the binding of the *trans*-acting tTR-KRAB fusion protein to

ular culture medium was added onto the transfected cells. At 3 days post-transfection, reporter-directed flow cytometry was carried out to establish the frequency of transfected cells in the various cultures. Subsequently, the cells were sub-cultured about every 3–4 days. In order to activate target gene expression, cultures of HEK.EGFP[TetO.KRAB] and HER.TLR[TetO.KRAB] cells were exposed to Dox at 10 and 14 days post-transfection, respectively. Reporter-directed flow cytometry was performed on HEK.EGFP[TetO.KRAB] and HER.TLR[TetO.KRAB] cells 7 and 10 days later, respectively. Where indicated, *TetO*-negative control HER.TLR[KRAB] cells were subjected to the same conditions as those applied to their HER.TLR[TetO.KRAB] counterparts.

Flow cytometry

The quantification of reporter-positive cells was done by a BD LSR II flow cytometer (BD Biosciences). The results were analyzed with the aid of BD FACSDiva 6.1.3 software (BD Biosciences) or FlowJo 7.2.2 software (Tree Star). Mock-transfected target cells were used to set background fluorescence. At least 10 000 viable single cells were analyzed per sample.

Chromatin immunoprecipitation (ChIP) and qPCR

The HER.TLR[TetO.KRAB] cells were cultured in the presence or in the absence of Dox (500 ng/ml) for 11 days, after which a cell fixation protocol available at https://www.activemotif.com, was applied. In brief, 2 ml of a freshly prepared formaldehyde solution was added into the cell culture medium. The culture flasks were subsequently agitated for exactly 15 min at room temperature. Next, 1.1 ml of 2.5 M glycine was applied to stop the fixation process. After a 5-min incubation period at room temperature, the cells were scraped and transferred to a 50-ml tube. The collected cells were subjected to two cycles of centrifugation at 800 ×*g* for 10 min. After the first cycle, the cells were resuspended in 10 ml of pre-chilled Igepal solution (0.05% Igepal in phosphate buffered saline (PBS)), whilst after the second cycle a 10 ml 0.05% Igepal solution mixed with 100 μl phenylmethanesulfonyl fluoride (Sigma P-7626, 100 mM in ethanol), was used instead. A final centrifugation at 800 ×*g* for 10 min was carried out to harvest the fixed cell pellets. Subsequently, the ChIP-qPCR assays were performed on 30 μg of cross-linked chromatin according to the HistonePath[TM] ChIP-qPCR protocol (Active Motif). The ChIP-validated antibodies H3 pan-acetyl (Active Motif, cat # 39139) and H3K9me3 (Active Motif, cat # 39161) were used for the ChIP. Next, qPCR amplifications with primer pairs (Supplementary Table S5) targeting six different *TLR*[TetO] regions (i.e. SFFV promoter, *EF1α* promoter, puromycin resistance gene, *mCherry* sequence, 5′ and 3′ *EGFP* gene segments) were performed. Additional primer pairs were used for the quality control of the ChIP-qPCR assays (Supplementary Table S5).

The qPCR amplifications were performed with the aid of a Bio-Rad CFX Connect Real-time detection system running the CFX Manager[TM] software. The qPCR amplifications were carried out in triplicate for each sample and primer pair. The qPCR mixtures consisted of 12.5 ng of input DNA, 1x iQ SYBR Green Supermix (Bio-Rad) and 250 nM of each primer in a total volume of 20 μl. The qPCR program started with a 2-min incubation period at 95°C. This was followed by 40 cycles consisting of 15 s at 95°C, 20 s at 58°C and 20 s at 72°C. Next, the samples were sequentially incubated at 95°C and 55°C for 1 min. The melting curves were derived by increasing the temperature from 55°C to 95°C with a rate of 0.5°C for every 10 s. The binding events detected per 1000 cells were calculated based on chromatin input amounts, final ChIP volumes and primer efficiencies. Finally, the data were normalized using the algorithm available at https://www.activemotif.com.

Statistical analysis

The comparison of data sets resulting from a minimum of three independent experiments were analyzed by using the GraphPad Prism 6 software package and monitored for significance by applying two-tailed Student's *t*-tests with $P < 0.05$ considered significant. The data sets derived from two independent experiments done in biological replicate in HER.TLR[KRAB] were analyzed by using the IBM SPSS Statistics 23 software package and monitored for significance by employing a three-way ANOVA test with $P < 0.05$ considered significant. One-way ANOVA combined with Bonferroni tests were used for the statistical analysis of the data corresponding to the screening of the high-specificity Cas9 variants. $P < 0.05$ was considered significant. The IBM SPSS Statistics 23 software package was used in this analysis.

---

cis-acting *TetO* sequences leads to the recruitment of epigenetics modulators consisting of, amongst others, KAP1 and HP1 proteins. In the presence of doxycycline, tTR-KRAB cannot bind its cognate *TetO* elements, resulting in the transition of a compact heterochromatic to a relaxed euchromatic conformation. (**B**) Designer nuclease-induced gain-of-function system (ORF correction). HER.TLR[TetO.KRAB] reporter cells contain a *TetO*-flanked *TLR* allele. Subjecting tTR-KRAB-expressing HER.TLR[TetO.KRAB] cells to designer nucleases targeting *TLR* sequences yields ORF-correcting indels generated by NHEJ-mediated DSB repair and the appearance of mCherry-positive cells. (**C**) ChIP-qPCR analysis on HER.TLR[TetO.KRAB] cells. ChIP-qPCR signals detected by using antibodies directed against open and closed chromatin marks (H3Ac and H3K9me3, respectively). Six different regions spanning the *TLR*[TetO] gene body were probed. The targeted sequences were located in the *EF1α* promoter (EF1α), the *puromycin resistance* ORF (Puro[R]), the spleen focus-forming virus regulatory elements (SFFV), the *EGFP* ORF (EGFP a and EGFP b) and the *mCherry* ORF (mCherry). Standard positive and negative controls (Ctrl) are indicated. (**D**) Designer nuclease-induced loss-of-function system (ORF disruption). HEK.EGFP[TetO.KRAB] reporter cells harbor a *TetO*-flanked *EGFP* target allele. Exposing tTR-KRAB-expressing HEK.EGFP[TetO.KRAB] cells to designer nucleases targeting *EGFP* yields ORF-disrupting indels generated by NHEJ DSB repair and the emergence of EGFP-negative cells. (**E**) Experimental settings. HEK.EGFP[TetO.KRAB] and HER.TLR[TetO.KRAB] cells exposed or not to Dox are transfected with designer nuclease-encoding constructs. After the generation of site-specific DSBs and ensuing NHEJ-mediated indel formation in each of the two parallel settings (yellow boxes), target gene expression is activated allowing to quantify the frequencies of NHEJ-based gene editing by flow cytometry.
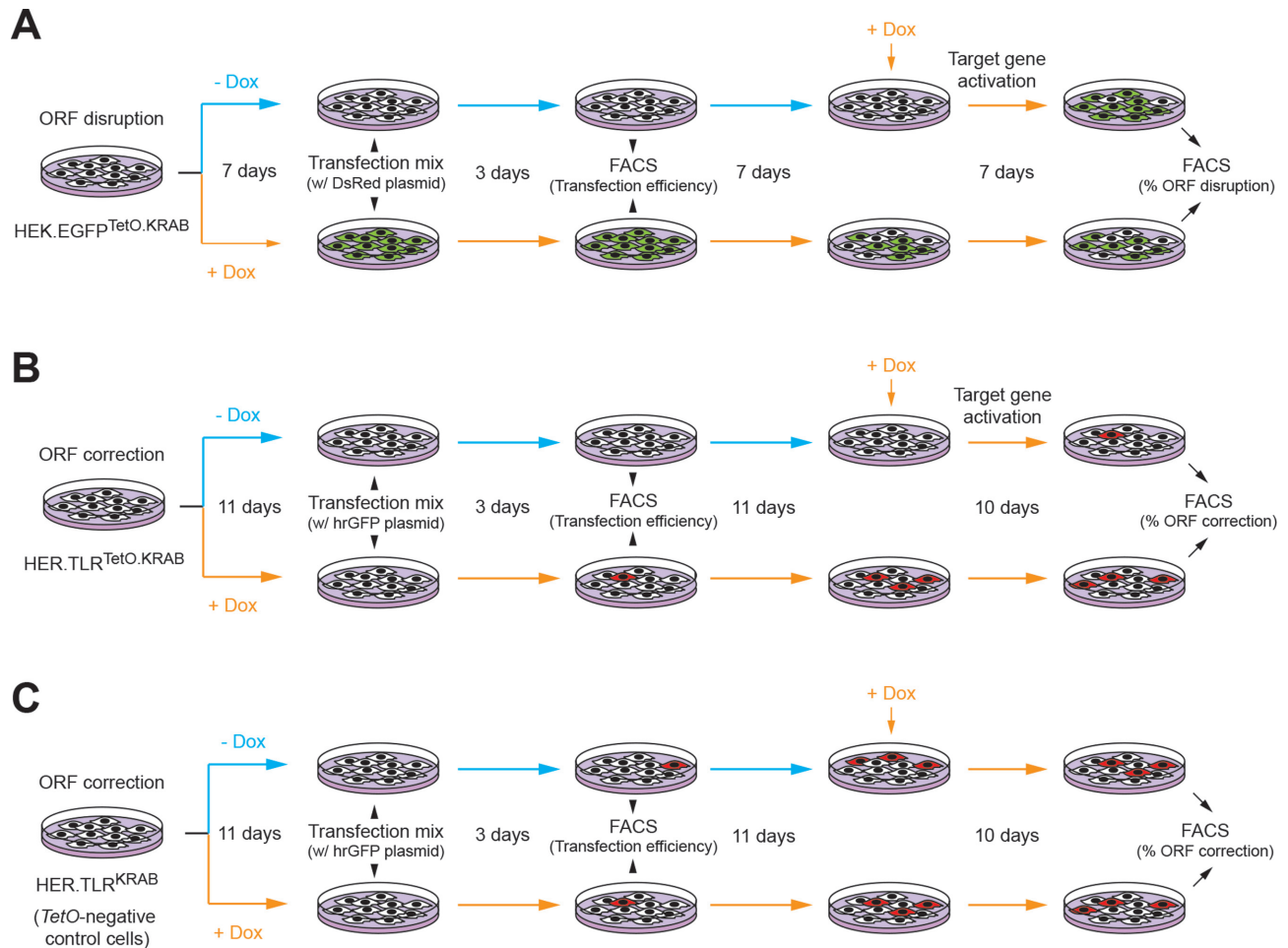
Figure 2. Detailed diagrammatic representation of the experimental designs used in the present study. The tTR-KRAB-expressing reporter cells HEK.EGFP$^{TetO.KRAB}$(**A**) and HER.TLR$^{TetO.KRAB}$ (**B**) were used for tracking and quantifying designer nuclease-induced gene editing events at target sites subjected to different epigenetic states. The *TetO*-negative and tTR-KRAB-expressing reporter cells HER.TLR^{KRAB}(**C**) were also generated to provide for negative controls. The HEK.EGFP$^{TetO.KRAB}$ and HER.TLR$^{TetO.KRAB}$ systems are complementary in that they allow for measuring ORF disruption and ORF correction, respectively. The initial high-order chromatin conformation of both model alleles is controlled through Dox-dependent regulation of tTR-KRAB binding. Reporter cells HEK.EGFP$^{TetO.KRAB}$ and HER.TLR$^{TetO.KRAB}$, containing target sequences in a heterochromatic (–Dox) or euchromatic (+Dox) state, are transiently transfected with different sets of designer nuclease-encoding constructs. DsRed and hrGFP expression plasmids are included in the transfection mixtures to serve as internal controls for transfection efficiency. After the generation of targeted DSBs in each of the two parallel settings (i.e. –Dox and +Dox), target gene expression is activated allowing to quantifying the frequencies of NHEJ-based gene editing by flow cytometry.

RESULTS AND DISCUSSION

To investigate and compare the impact that the chromatin structure has on the performance of TALENs and CRISPR-Cas9 complexes, we have set-up two complementary quantitative cellular systems dubbed HER.TLR$^{TetO.KRAB}$ and HEK.EGFP$^{TetO.KRAB}$. In these systems, the chromatin conformations (i.e. euchromatic versus heterochromatic) at isogenic target sequences are stringently controlled through small-molecule drug availability. In particular, these experimental models based on human cells, harbor reporter alleles whose transition from compact to relaxed chromatin is governed through doxycycline (Dox)-dependent release of a dominantly silencing tTR-KRAB fusion protein from its cognate *TetO* recognition elements (Figure 1A). The Krüppel-associated box domain (KRAB) is the effector moiety of the largest

class of transcriptional repressors in vertebrates. The binding of KRAB-containing proteins to DNA triggers epigenetic silencing mechanisms involving the recruitment of, amongst others, scaffolding and chromatin remodeling factors such as KRAB-associated protein 1 (KAP-1) and heterochromatin protein 1 (HP-1) (27,28). The impinged facultative heterochromatin is characterized by epigenetic marks of silenced genes (29,30).

The first system, HER.TLR$^{TetO.KRAB}$, consists of tTR-KRAB-expressing human embryonic retinoblasts containing a Traffic Light Reporter (*TLR*) construct (12), which we have herein modified by flanking it with *TetO* (*TLR*^{TetO}) elements (Figure 1B). The original *TLR* construct has an out-of-frame *mCherry* reporter located downstream of a T2A sequence and an *EGFP* ORF disrupted by an I-SceI recognition site (12). The repair by NHEJ of DSBs made at sequences upstream of *mCherry* generates indels that can
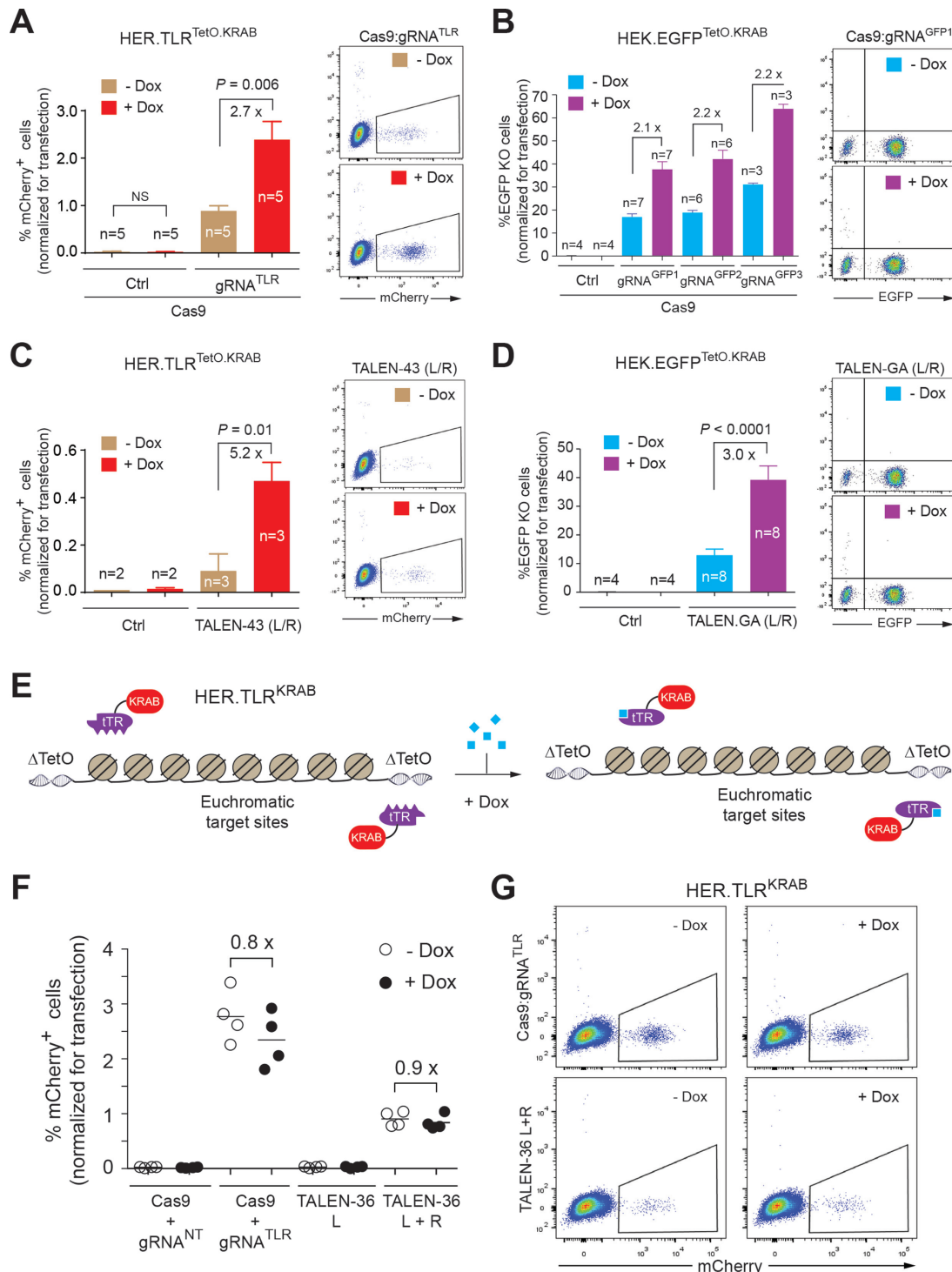
Figure 3. The impact of distinct chromatin conformations on the frequencies of NHEJ-based gene editing achieved by TALEN and CRISPR/Cas9 nucleases. Reporter cells HER.TLR[TetO.KRAB] (**A** and **C**) and HEK.EGFP[TetO.KRAB] (**B** and **D**), were subjected to the indicated experimental conditions. The negative controls (Ctrl) in panels **A** and **B**, involved transfecting cells with expression plasmids encoding Cas9 mixed with a non-targeting gRNA or with an 'empty' gRNA construct, respectively. The negative controls (Ctrl) in panel **C** and in panel **D** involved exposing target cells exclusively to a single TALEN monomer. Representative flow cytometry dot plots are also presented next to each graph. Ten thousand events, each corresponding to a single viable cell, were measured per sample. Error bars indicated mean ± s.e.m. *P* values (by two-tailed *t*-tests) and the number of independent experiments (*n*) are shown. (**E**) Control HER.TLR[KRAB] cells. The chromatin status of *TLR* sequences in HER.TLR[KRAB] cells are not controlled by Dox since they lack *cis*-acting *TetO* elements for tTR-KRAB binding. (**F**) Gene editing in HER.TLR[KRAB] cells. HER.TLR[KRAB] cells were either exposed or not to Dox and were subsequently transfected with the indicated constructs. Differences between +Dox and –Dox values were not statistically significant as determined by three-way ANOVA (*P* = 0.151; two independent experiments done in replicate). The ratios between *EGFP* knockout levels measured in the presence versus those determined in the absence of Dox. gRNA[NT], Non-targeting gRNA. (**G**) Representative flow cytometry dot plots corresponding to the experimental settings presented in panel **F**.
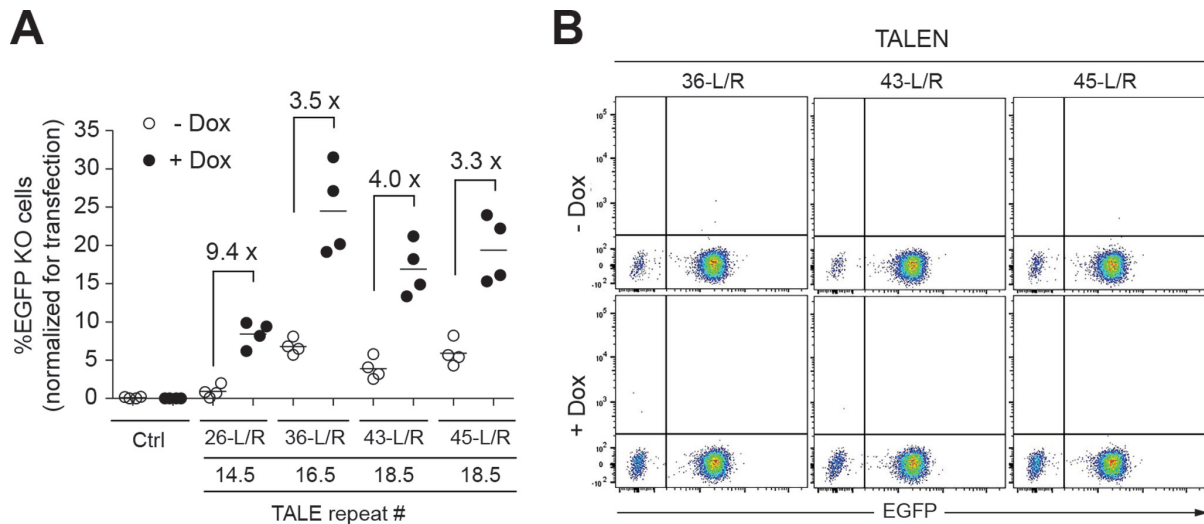
Figure 4. Gene editing experiments at *EGFP* target sequences subjected to alternative chromatin conformations. (**A**) Targeted mutagenesis induced by TALENs with different numbers of TALE repeats. HEK.EGFP$^{TetO.KRAB}$ cells were either incubated or not with Dox and were subsequently transfected with expression plasmids encoding TALENs with 14.5, 16.5 and 18.5 TALE repeats. Negative controls consisted of parallel cultures exposed exclusively to TALEN-GA-L (Ctrl). After the generation of site-specific DSBs in each of the two parallel settings (i.e. -Dox and +Dox), target gene expression was activated in all cultures by adding Dox for determining the frequencies of NHEJ-mediated *EGFP* knockout by flow cytometry. The ratios between *EGFP* knockout levels measured in the presence versus those determined in the absence of Dox (open versus closed chromatin, respectively) are indicated. (**B**) Representative flow cytometry dot plots corresponding to the experimental settings presented in panel **A**.

place the nucleotide sequence of *mCherry* in-frame. The resulting red fluorescent cells thus report sequence-specific nuclease activity. To validate the cellular model based on the adapted *TLR* construct *TLR*^{TetO}, ChIP-qPCR assays were performed on HER.TLR$^{TetO.KRAB}$ cells incubated in the presence or in the absence of Dox. In these assays, antibodies directed against histone 3 acetylation (H3Ac) and histone 3 lysin 9 trimethylation (H3K9me3), characteristic of open and closed chromatin, respectively, were used. The ChIP-qPCR analysis established a Dox-dependent switch of *TLR*^{TetO} sequences from a heterochromatic to a euchromatic state (Figure 1C). Indeed, in HER.TLR$^{TetO.KRAB}$ cells not exposed to Dox, the enrichment factors for the heterochromatin mark H3K9me3 at six randomly-selected ChIP-qPCR target regions spanning the *TLR*^{TetO} gene body varied from a minimum of 2.2-fold to a maximum of 14.4-fold when compared to those measured in their Dox-treated counterparts (Figure 1C, left panel). Conversely, in HER.TLR$^{TetO.KRAB}$ cells exposed to Dox, the enrichment factors for the euchromatin mark H3Ac at the same ChIP-qPCR target regions ranged from a minimum of 1.1-fold to a maximum of 61.7-fold when compared to those measured in their Dox-negative counterparts (Figure 1C, right panel). These variations in histone modifications are well within those reported to induce biologically relevant changes in cells (30,31). Taken together, these data validate the *TLR*^{TetO} construction as a Dox-dependent epigenetically controlled system that can be used for studying the effect of chromatin conformation on the performance of gene editing tools. The second system, HEK.EGFP$^{TetO.KRAB}$, entails tTR-KRAB-expressing human embryonic kidney cells with a *TetO*-flanked functional *EGFP* allele (12) (Figure 1D). In this system, the traceable cellular phenotype consists of non-fluorescent cells emerging from the incorporation of frame-shifting indels at *EGFP* sequences after

NHEJ-mediated DSB repair. In conclusion, the generation of DSBs within isogenic euchromatic and heterochromatic target sites located in *TLR* and *EGFP* reporter genes can readily be tracked *in cellula* by quantifying mCherry-positive and EGFP-negative cells, respectively (Figure 1E).

We started by transfecting HER.TLR$^{TetO.KRAB}$ and HEK.EGFP$^{TetO.KRAB}$ cells, cultured in the presence or in the absence of Dox, with expression plasmids encoding TALENs and CRISPR/Cas9 nucleases (Supplementary Figure S5). Parallel cell cultures transfected with constructs expressing a single TALEN monomer, Cas9 plus a non-targeting gRNA or Cas9 plus an 'empty' gRNA, served as negative controls (Ctrl). After the action of the various designer nucleases had taken place, all cell cultures were exposed to Dox in order to allow for transgene activation and ensuing flow cytometric analysis (Figures 1E and 2). The resulting data revealed that in HER.TLR$^{TetO.KRAB}$ and HEK.EGFP$^{TetO.KRAB}$ cells (i.e. ORF correction and ORF disruption readouts, respectively), the frequencies of DSB formation were significantly lower in cells whose target sites were embedded in heterochromatin (-Dox) when compared to those attained when the same sites were located in euchromatin (+Dox) instead (Figure 3A–D and Supplementary Figure S6). Indeed, euchromatic target sequences in reporter HER.TLR$^{TetO.KRAB}$ and HEK.EGFP$^{TetO.KRAB}$ cells were cleaved by CRISPR/Cas9 complexes on average 2.7- and 2.2-fold, more frequently than when they were in a heterochromatic state (Figure 3A and B, respectively). Similarly, euchromatic target sites in reporter HER.TLR$^{TetO.KRAB}$ and HEK.EGFP$^{TetO.KRAB}$ cells were cut by TALEN dimers on average 5.2- and 3.0-fold more often than their isogenic heterochromatic counterparts (Figure 3C and D, respectively). Thus, these ratios between the levels of targeted DSB formation in epigenetically open versus closed DNA can be
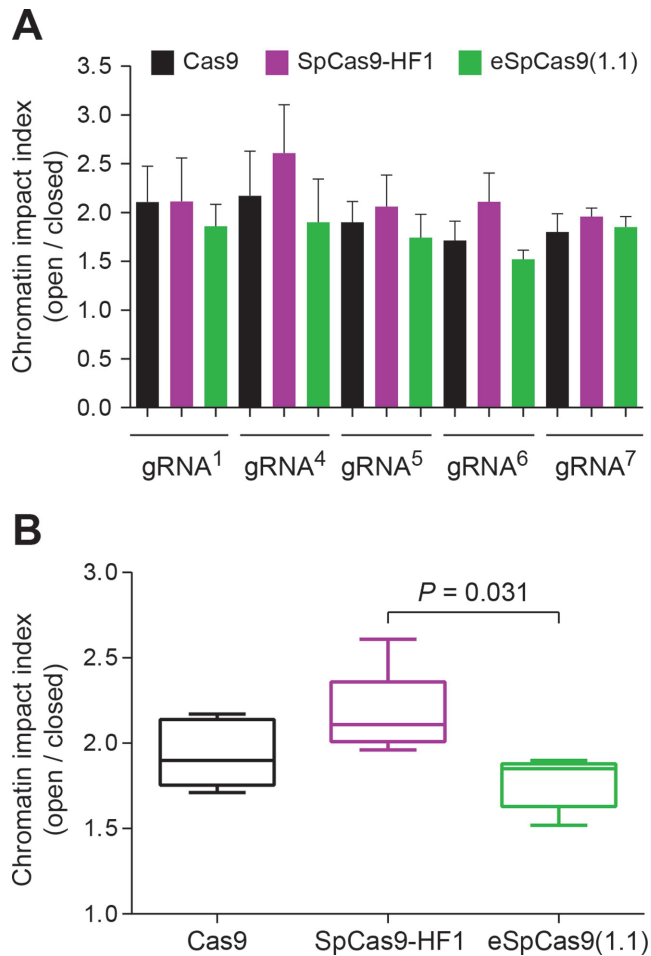
A

B

Figure 5. Testing the impact of chromatin conformation on high-specificity Cas9 variants. (**A**) Screening of CRISPR/Cas9 complexes with different Cas9 proteins in HEK.EGFP[TetOKRAB] cells. HEK.EGFP[TetOKRAB] cells were incubated in the presence or in the absence of Dox and were subsequently transfected with expression plasmids encoding the indicated CRISPR/Cas9 nuclease components. The chromatin impact index was determined by computing the ratios between *EGFP* knockout levels measured in the presence versus those determined in the absence of Dox. Error bars indicate mean ± s.e.m. corresponding to three independent experiments. Ten thousand events, each corresponding to a single viable cell, were measured per sample. (**B**) Cumulative chromatin impact indexes. Boxplot of the chromatin impact indexes presented in panel **A**. Whiskers, minimum and maximum. One-way ANOVA compared the experimental groups with a subsequent comparison between groups being done by Bonferroni analysis ($P < 0.05$ was considered significant).

referred to as the chromatin impact index of a particular nuclease.

Of note, the TALEN pairs TALEN-43-L/TALEN-43-R and TALEN-GA-L/TALEN-GA-R (Figure 3C and D, respectively) are based on different architectures consisting of TALE scaffolds from *Xanthomonas axonopodis pv. citri* and *Xanthomonas campestris pv. armoraciae*, respectively (32,33). Importantly, no differences in designer nuclease-induced targeted DSB frequencies were measured in HER.TLR[KRAB] cells whose *TLR* sequences are not subjected to conditional KRAB-mediated epigenetic regulation (Figure 3E). HER.TLR[KRAB] and HER.TLR[TetO.KRAB]
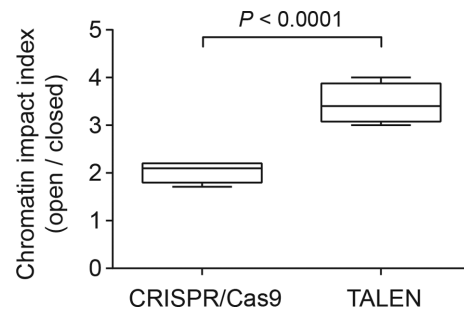

Figure 6. Cumulative chromatin impact indexes for the TALEN and CRISPR/Cas9 nuclease systems. Boxplot of the ratios between *EGFP* knockout levels measured in the presence versus those determined in the absence of Dox presented in Figures 3B, D, 4A and 5B (Cas9 data points). Whiskers, minimum and maximum. The data corresponding to the TALEN pair with the shortest DNA-binding domains (i.e. TALEN-26-L/TALEN-26-R) was not computed in this analysis to avoid skewing the data. Ten thousand events, each corresponding to a single viable cell, were measured per sample. The *P*-value was determined by two-tailed Student's *t*-test analysis ($P < 0.05$ was considered significant).

cells differ from each other in that the former lacks the *cis*-acting *TetO* elements (Figures 1A and 3E, respectively). In particular, expression of TALEN dimers and CRISPR/Cas9 complexes directed to *TLR* sequences in HER.TLR[KRAB] cells led to similar levels of site-specific DSB formation in Dox-containing and Dox-free settings resulting in chromatin impact indexes of roughly 1 for both types of designer nucleases (Figure 3F and G).

Next, we carried out another series of gene knockout experiments in HEK.EGFP[TetO.KRAB] cells by using a panel of TALENs composed of different numbers of TALE repeats in their DNA-binding arrays. Once again, the frequencies of targeted gene knockout were highest in cells containing euchromatic target sites (Figure 4A and B). Interestingly, the TALEN complex built on monomers with the shortest TALE DNA-binding domains was the most hindered by having its target sequence embedded in heterochromatin. In fact, under this condition, this TALEN pair led to gene editing levels barely above background (Figure 4A). These data suggest that a minimum TALEN DNA-binding energy is necessary in order to overcome the compact heterochromatic barrier and induce meaningful levels of site-specific DSB formation. Nonetheless, it is important to point out that the majority of TALEN proteins currently in use contain DNA-binding domains made up of well over 14.5 TALE repeats (i.e. typically, 17.5 to 18.5 TALE repeats per monomer) (1,2).

Informed by structural data (4,34), two independent research groups have recently generated *S. pyogenes* Cas9 variants with targeting DNA specificities markedly superior to that of their parental wild-type counterpart (19,21). These high-specificity variants, dubbed SpCas9-HF1 (19) and eSpCas9(1.1) (21), have amino acid substitutions which reduce nonspecific protein–DNA interactions and, as a result, constrain the respective ribonucleoprotein complexes to preferentially cut at the intended target sites. The SpCas9-HF1 mutations N497A, R661A, Q695A and Q926A reduce protein binding to the sugar-phosphate backbone of the complementary strand by removing hy-

drogen bridges; the charged-to-alanine eSpCas9(1.1) mutations K848A, K1003A and R1060A affect protein binding to the non-complementary stand by eliminating cationic amino acids along the nt-groove located between the HNH and RuvC-like nuclease domains. Regardless of their different point mutations and *modus operandi*, these engineered Cas9 variants contribute to addressing in a very direct manner a major issue in the genome-editing field, that is, the need for reducing off-target DNA cleaving activities as these can confound experimental outcomes and obstruct potential clinical applications. To determine the relative chromatin impact indexes of these new Cas9 variants, we carried out targeted gene knockout experiments in HEK.EGFP$^{TetO.KRAB}$ cells. In these experiments, constructs encoding wild-type Cas9, SpCas9-HF1 or eSpCas9(1.1) were transfected together with plasmids expressing five different *EGFP*-targeting gRNAs. Data presented in Figure 5A show that, as previously established for wild-type Cas9, high-specificity Cas9 variants were both hindered by heterochromatin. Interestingly, of the two variants, the SpCas9-HF1 protein was the most affected in these experiments as indicated by its higher chromatin impact index (Figure 5B).

Taken together, our data establishes that distinct high-order epigenetically regulated chromatin conformations can have a significant impact on DNA cleaving activity regardless of the type of the designer nuclease tested and of the specific nucleotide sequence targeted. Moreover, of the two main designer nuclease platforms currently in use, TALENs seem to be the most influenced by the high-order chromatin status of their target DNA as revealed by the cumulative data presented in Figure 6. In this regard, it is interesting noting that although the RNA-guided system has not evolved to assess and cleave chromosomal DNA in eukaryotic cell nuclei, it can nonetheless perform relatively well in human cells when compared to TALENs (Figure 6). However, regardless of the nuclease platform ultimately chosen, chromatin impact indexes of two or higher (Figure 6) are relevant for the ultimate performance of genome editing protocols in different experimental settings, including those aiming at bi-allelic or multi-allelic target gene knockouts. Our results complement recent biochemical data demonstrating that nucleosome occupancy obstructs CRISPR/Cas9-mediated DNA cleavage (35). Interestingly, comparison of targeted DSB formation by TALENs and CRISPR/Cas9 nucleases at different *CCR5* sequences in induced pluripotent stem cells did not show a correlation between indel frequencies and the distribution of DNaseI hypersensitive sites retrieved from the ENCODE database (36). Whether this finding is specific to the DNaseI hypersensitive site profile selected or to the experimental design used, would need further investigation.

In the present work, we have presented and validated two complementary functional readouts for investigating and comparing in a quantitative manner the role of high-order chromatin structures on genome editing events resulting from the use of sequence-specific designer nucleases. By using these quantitative assays, we have demonstrated that TALENs and CRISPR/Cas9 nucleases are both significantly hindered by closed chromatin in living cells. We conclude that, in addition to the well-established parameters mentioned earlier, the chromatin conformation con-

stitutes yet another determinant of the ultimate efficiencies resulting from using TALENS and CRISPR/Cas9 nucleases. The approaches described in our work should be directly applicable for screening and selecting specific designer nuclease reagents from different platforms or with different architectures and compositions (e.g. hybrid nucleases, engineered homing endonucleases, Cas9 orthologues, novel Cas9 variants and gene editing tools co-opted from new DNA-targeting systems). In addition, they should also be valuable for assessing the impact of chromatin on different gene editing strategies, including those based on paired 'nickases', truncated guide RNAs and homology-directed gene repair.

SUPPLEMENTARY DATA

Supplementary Data are available at NAR Online.

REFERENCES

1. Kim,H. and Kim,J.-S. (2014) A guide to genome engineering with programmable nucleases. *Nat. Rev. Genet.*, **15**, 321–334.
2. Maggio,I. and Gonçalves,M.A.F.V. (2015) Genome editing at the crossroads of delivery, specificity, and fidelity. *Trends. Biotechnol.*, **33**, 280–291.
3. Chylinski,K., Makarova,K.S., Charpentier,E. and Koonin,E.V. (2014) Classification and evolution of type II CRISPR-Cas systems. *Nucleic Acids Res.*, **42**, 6091–6105.
4. Anders,C., Niewoehner,O., Duerst,A. and Jinek,M. (2014) Structural basis of PAM-dependent target DNA recognition by the Cas9 endonuclease. *Nature*, **513**, 569–573.
5. Chen,S., Oikonomou,G., Chiu,C.N., Niles,B.J., Liu,J., Lee,D.A., Antoshechkin,I. and Prober,D.A. (2013) A large-scale in vivo analysis reveals that TALENs are significantly more mutagenic than ZFNs generated using context-dependent assembly. *Nucleic Acids Res.*, **41**, 2769–2778.
6. Valton,J., Dupuy,A., Daboussi,F., Thomas,S., Maréchal,A., Macmaster,R., Melliand,K., Juillerat,A. and Duchateau,P. (2012) Overcoming Transcription Activator-like Effector (TALE) DNA binding domain sensitivity to cytosine methylation. *J. Biol. Chem.*, **287**, 38427–38432.
7. Wu,X., Kriz,A.J. and Sharp,P.A. (2014) Target specificity of the CRISPR-Cas9 system. *Quant. Biol.*, **2**, 59–70.
8. Kuscu,C., Arslan,S., Singh,R., Thorpe,J. and Adli,M. (2014) Genome-wide analysis reveals characteristics of off-target sites bound by the Cas9 endonuclease. *Nat. Biotechnol.*, **32**, 677–683.
9. O'Geen,H., Henry,I.M., Bhakta,M.S., Meckler,J.F. and Segal,D.J. (2015) A genome-wide analysis of Cas9 binding specificity using ChIP-seq and targeted sequence capture. *Nucleic Acids Res.*, **43**, 3389–3404.

10. Polstein,L.R., Perez-Pinera,P., Kocak,D.D., Vockley,C.M., Bledsoe,P., Song,L., Safi,A., Crawford,G.E., Reddy,T.E. and Gersbach,C.A. (2015) Genome-wide specificity of DNA binding, gene regulation, and chromatin remodeling by TALE- and CRISPR/Cas9-based transcriptional activators. *Genome Res.*, **25**, 1158–1169.

11. Wu,X., Scott,D.A., Kriz,A.J., Chiu,A.C., Hsu,P.D., Dadon,D.B., Cheng,A.W., Trevino,A.E., Konermann,S., Chen,S. *et al.* (2014) Genome-wide binding of the CRISPR endonuclease Cas9 in mammalian cells. *Nat. Biotechnol.*, **32**, 670–676.

12. Certo,M.T., Ryu,B.Y., Annis,J.E., Garibov,M., Jarjour,J., Rawlings,D.J. and Scharenberg,A.M. (2011) Tracking genome engineering outcome at individual DNA breakpoints. *Nat. Methods*, **8**, 671–676.

13. Szulc,J., Wiznerowicz,M., Sauvain,M.-O., Trono,D. and Aebischer,P. (2006) A versatile tool for conditional gene expression and knockdown. *Nat. Methods*, **3**, 109–116.

14. Reyon,D., Tsai,S.Q., Khayter,C., Foden,J.A., Sander,J.D. and Joung,J.K. (2012) FLASH assembly of TALENs for high-throughput genome editing. *Nat. Biotechnol.*, **30**, 460–465.

15. Holkers,M., Maggio,I., Henriques,S.F., Janssen,J.M., Cathomen,T. and Gonçalves,M.A. (2014) Adenoviral vector DNA for accurate genome editing with engineered nucleases. *Nat. Methods*, **11**, 1051–1057.

16. Mali,P., Yang,L., Esvelt,K.M., Aach,J., Guell,M., DiCarlo,J.E., Norville,J.E. and Church,G.M. (2013) RNA-Guided Human Genome Engineering via Cas9. *Science*, **339**, 823–826.

17. Kearns,N.A., Genga,R.M.J., Enuameh,M.S., Garber,M., Wolfe,S.A. and Maehr,R. (2013) Cas9 effector-mediated regulation of transcription and differentiation in human pluripotent stem cells. *Development*, **141**, 219–223.

18. Chapdelaine,P., Moisset,P.-A., Campeau,P., Asselin,I., Vilquin,J.-T. and Tremblay,J.P. (2000) Functional EGFP–dystrophin fusion proteins for gene therapy vector development. *Protein Eng.*, **13**, 611–615.

19. Kleinstiver,B.P., Pattanayak,V., Prew,M.S., Tsai,S.Q., Nguyen,N.T., Zheng,Z. and Joung,J.K. (2016) High-fidelity CRISPR-Cas9 nucleases with no detectable genome-wide off-target effects. *Nature*, **529**, 490–495.

20. Fu,Y., Sander,J.D., Reyon,D., Cascio,V.M. and Joung,J.K. (2014) Improving CRISPR-Cas nuclease specificity using truncated guide RNAs. *Nat. Biotechnol.*, **32**, 279–284.

21. Slaymaker,I.M., Gao,L., Zetsche,B., Scott,D.A., Yan,W.X. and Zhang,F. (2016) Rationally engineered Cas9 nucleases with improved specificity. *Science*, **351**, 84–88.

22. Maggio,I., Stefanucci,L., Janssen,J.M., Liu,J., Chen,X., Mouly,V. and Goncalves,M.A. (2016) Selection-free gene repair after adenoviral vector transduction of designer nucleases: rescue of dystrophin synthesis in DMD muscle cell populations. *Nucleic Acids Res.*, **44**, 1449–1470.

23. Pelascini,L.P. and Goncalves,M.A. (2014) Lentiviral vectors encoding zinc-finger nucleases specific for the model target locus HPRT1. *Methods. Mol. Biol.*, **1114**, 181–199.

24. Pelascini,L.P., Janssen,J.M. and Goncalves,M.A. (2013) Histone deacetylase inhibition activates transgene expression from integration-defective lentiviral vectors in dividing and non-dividing cells. *Hum. Gene Ther.*, **24**, 78–96.

25. Brielmeier,M., Béchet,J.M., Falk,M.H., Pawlita,M., Polack,A. and Bornkamm,G.W. (1998) Improving stable transfection efficiency: antioxidants dramatically improve the outgrowth of clones under dominant marker selection. *Nucleic Acids Res.*, **26**, 2082–2085.

26. Fallaux,F.J., Bout,A., van der Velde,I., van den Wollenberg,D.J., Hehir,K.M., Keegan,J., Auger,C., Cramer,S.J., van Ormondt,H., van der Eb,A.J. *et al.* (1998) New helper cells and matched early region 1-deleted adenovirus vectors prevent generation of replication-competent adenoviruses. *Hum. Gene Ther.*, **9**, 1909–1917.

27. Lechner,M.S., Begg,G.E., Speicher,D.W. and Rauscher,F.J. (2000) Molecular determinants for targeting heterochromatin protein 1-mediated gene silencing: direct chromoshadow domain–KAP-1 corepressor interaction is essential. *Mol. Cell. Biol.*, **20**, 6449–6465.

28. Nielsen,A.L., Ortiz,J.A., You,J., Oulad-Abdelghani,M., Khechumian,R., Gansmuller,A., Chambon,P. and Losson,R. (1999) Interaction with members of the heterochromatin protein 1 (HP1) family and histone deacetylation are differentially involved in transcriptional silencing by members of the TIF1 family. *EMBO J.*, **18**, 6385–6395.

29. Ayyanathan,K., Lechner,M.S., Bell,P., Maul,G.G., Schultz,D.C., Yamada,Y., Tanaka,K., Torigoe,K. and Rauscher,F.J. (2003) Regulated recruitment of HP1 to a euchromatic gene induces mitotically heritable, epigenetic gene silencing: a mammalian cell culture model of gene variegation. *Genes Dev.*, **17**, 1855–1869.

30. Groner,A.C., Meylan,S., Ciuffi,A., Zangger,N., Ambrosini,G., Denervaud,N., Bucher,P. and Trono,D. (2010) KRAB-zinc finger proteins and KAP1 can mediate long-range transcriptional repression through heterochromatin spreading. *PLoS Genet.*, **6**, e1000869.

31. Becker,J.S., Nicetto,D. and Zaret,K.S. (2016) H3K9me3-Dependent Heterochromatin: Barrier to cell fate changes. *Trends Genet.*, **32**, 29–41.

32. Mahfouz,M.M., Li,L., Shamimuzzaman,M., Wibowo,A., Fang,X. and Zhu,J.K. (2011) De novo-engineered transcription activator-like effector (TALE) hybrid nuclease with novel DNA binding specificity creates double-strand breaks. *Proc. Natl. Acad. Sci. U.S.A.*, **108**, 2623–2628.

33. Miller,J.C., Tan,S., Qiao,G., Barlow,K.A., Wang,J., Xia,D.F., Meng,X., Paschon,D.E., Leung,E., Hinkley,S.J. *et al.* (2011) A TALE nuclease architecture for efficient genome editing. *Nat. Biotech.*, **29**, 143–148.

34. Nishimasu,H., Ran,F.A., Hsu,P.D., Konermann,S., Shehata,S.I., Dohmae,N., Ishitani,R., Zhang,F. and Nureki,O. (2014) Crystal structure of Cas9 in complex with guide RNA and target DNA. *Cell*, **156**, 935–949.

35. Horlbeck,M.A., Witkowsky,L.B., Guglielmi,B., Replogle,J.M., Gilbert,L.A., Villalta,J.E., Torigoe,S.E., Tjian,R. and Weissman,J.S. (2016) Nucleosomes impede Cas9 access to DNA in vivo and in vitro. *ELife*, **5**, e12677.

36. Yang,L., Guell,M., Byrne,S., Yang,J.L., De Los Angeles,A., Mali,P., Aach,J., Kim-Kiselak,C., Briggs,A.W., Rios,X. *et al.* (2013) Optimization of scarless human stem cell genome editing. *Nucleic Acids Res.*, **41**, 9049–9061.